Fault Classification from 3D Imaging of a Vertical DAS Profile

Whitney Trainor-Guitton[*1], *Samir Jreij*[1], *Antoine Guitton*[2], *James Simmons*[1]
[1]*Colorado School of Mines,*[2]*DownUnder GeoSolutions*

SUMMARY

Faults play an important role in geothermal fluid transport and can also present a contrast in acoustic impedance such that seismic methods can approximately locate their presence in the subsurface. Brady Natural Lab is a geothermal reservoir that has numerous faults that allow for both recharge and deep-to-shallow heat exchange via subsurface fluids. In March 2016 at Brady, a continuous active seismic survey collected 191 3-mode vibe points, while a vertical DAS cable was in place 150 to 280 meters below surface. Imaging of both synthetic and field data was performed to analyze if certain fault dips and strikes would be detectable given the shot geometry. Bright spots exist that are consistent with 3 faults: the fault farthest from the DAS well at distance of 750m to the northeast, and two Western-dipping faults below the well that contains the DAS. Lastly, convolution neural networks were used to obtain an agnostic, quantitative measure of the reliability of detecting faults from images derived from DAS. A transfer learning approach utilized layers of convolutional neural networks trained on the ImageNet repository.

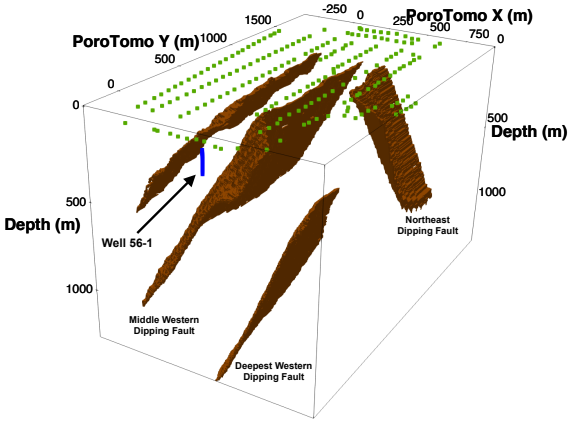

Figure 1: Southern view of 3D rendering of Bradys 4 fault model; Green dots are vibe points; blue line is location of vertical DAS well (Well 56-1A). The 3 faults are shown in Figures 3a and 3b.

INTRODUCTION

A power plant has operated for approximately 25 years at Brady Natural Lab where both artificial and natural recharge keep the reservoir pressurized (Cardiff et al., 2018; Folsom et al., 2018, Feigl et al., 2018). A vibrating source injected the 3 modes (P, transverse S, and longitudinal S) at 191 source locations during four stages of the 15-day field experiment. The four stages describe different production and injection regimes performed during the experiment: 1) normal production/injection, 2) production/injection stopped, 3) increased injection and pulsing production and 4) normal production/injection. The vibroseis truck operated in synchronization with the DAS array and the conventional seismometers. For each of the three modes, the vibroseis source made three sweeps over 20 seconds. Each sweep increased in frequency from 5 Hz to 80 Hz. To record the reflected and diffracted energy from these sources, there were 238 5Hz 3-component geophones, 8,700 meters of horizontal DAS cable (buried in a shallow trench) and 150-280 meters of DAS cable hanging vertically in Well 56-1, whose location is depicted by the blue line in Figure 1.

The coupling of the fiber downhole can vary depending on if the fiber is installed behind casing or in tubing (Raterman et al., 2017). Specifically, this paper focuses on understanding the vertical DAS (DASV) data and the extent to which DASV can be used for imaging of the steeply dipping faults. The DASV have potential to be more sensitive to the faults than the horizontal DAS and surface geophones, which given the acquisition geometry are prone to spatial aliasing (Jreij et al., 2018). However, DASV are only recorded in Well 56-1 location, and unfortunately, the fiber is not securely coupled to the casing but is hanging freely (Feigl et al., 2017). However, the frictional coupling allowed for reflection signals to be detected, similar to what is seen and described in Munn et al. (2017) and Lindsey et al. (2017). Both Trainor-Guitton et al. (2018) and Miller and Coleman (2018) describe the reflection events detected in the Brady vertical DAS dataset. We use convolutional neural networks (CNN) trained with the ImageNet (Russakovsky et al., 2015) and our fault images created with reverse-time migration of synthetic and field observations to quantitatively assess how well vertical DAS cable can properly locate the faults.

REVERSE TIME MIGRATION

In this abstract, we are probing the DAS data for information about the faults that play an important role in the circulation (recharge and upflow) of geothermal fluids. A contrast in impedance is expected given there is 10 meters and greater offset from the faulting at Brady (Queen et al., 2017). Given the southern location of the DAS fiber and the single component sensitivity of the DAS fiber (Mateeva et al., 2014; Daley et al., 2016), imaging will suffer from poor illumination and hence migration artifacts. Additionally, the velocity model used, described in Matzel et al. (2017), is highly uncertain (Feigl et al., 2018; Trainor-Guitton et al., 2018). Despite these challenges, we use reverse time migration and the Brady fault model (Siler and Faulds, 2013) as a reflectivity to begin to explain the DAS signals in terms of the geothermal reservoir faulting. RTM is one possible approach as the DASV data exhibits mode con-

versions. Migration methods are capable of simulating wave propagation in complex earth models, thus accounting for scattering and mode conversions.

All migration algorithms (reverse time migration here) image single scattering events, either reflections or diffractions. These algorithms are based on the Born approximation and decompose the medium into a background model responsible for travel time (i.e. velocity), and a perturbation model responsible for the reflections and diffractions (i.e. reflectivity)(Woodward, 1992). Theoretically, with a dense grid of source and receiver offsets, there is enough azimuthal and angle coverage to see diffractions and reflections. The migration used here is based on the imaging principle of Claerbout (1971), where a reflector exists when source and receiver wave fields coincide in space at zero time. Pre-stack depth migration code using the whole wavefield for each source and all receiver positions will give an accurate image of the subsurface if the velocity is correct and reflections and/or diffractions are present.

Flat reflectors: Sensitivity Test of Acquisition Geometry
Synthetic tests of four flat reflectors were first examined to help determine the volume of illumination and where to expect artifacts. Four horizontal reflectors (two constant velocity layers) are placed at depths of 750 m, 900 m, 1,150 m and 1,300 m respectively to demonstrate how much of the image is reliable given the reflection-point illumination coverage. Given the geometry of the sources, certain areas will not be probed by the vibe energy, and thus migration artifacts will dominate.

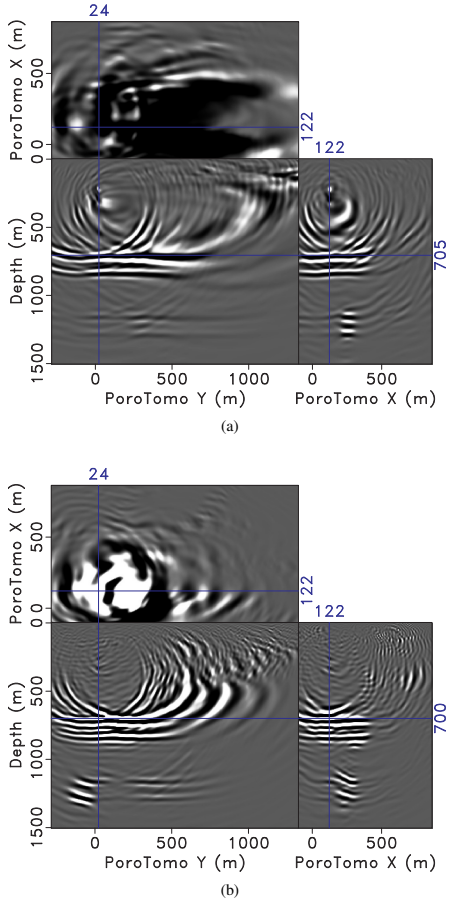

Figure 2: a) P-P image and b) P-S image of 4 flat reflectors using PoroTomo acquisition geometry

Figures 2a and 2b contain the two RTM images at the three orthogonal planes around the location of Well 56-1. Figure 2a is the imaging result using the p-wave velocity for the down and up-going, referred to as the P-P image. Figure 2b is the imaging result using the p-wave velocity for the down-going energy and the shear-wave velocity for the upgoing, referred to as the P-S image. RTM images are composed of a relative reflectivity, where both white and black are stronger magnitudes in images presented in this paper. Experienced interpreters look for, and identify, coherent structures or events in these images. For example, in Figures 2a and 2b we see the horizontal reflectors at locations that straddle the well location (about -100/+700 m in PoroTomo Y and +/-300 m in PoroTomo X in the P-P image). Beyond this, the image "structure" changes to a "migration smile" indicating poor illumination in that location of the model in these areas.

In addition to the source locations and velocity model, the images produced by RTM will be a function of the the DAS fiber sensitivity to particle motion in-line with the fiber. Jreij et al. (2018) demonstrates how horizontal DAS is more sensitive to P reflection events at large offsets (large emerging angles) and S events polarized vertically at short emerging angles, and S events polarized horizontally produced by a source that is perpendicular to the fiber orientation. This will be different for a vertical DAS and from reflections produced by steeply dipping faults.

Steeply Dipping Faults and Fiber Attributes
The 3D fault model of Brady (Siler and Faulds, 2013) was used as a reflectivity model along with the velocity model of Matzel et al. (2018). Images created from this combination are compared side-by-side with the RTM of the DASV data collected in the March 2016 field acquisition. Figures 3a and 3b are the P-P images of the same three orthogonal cross sections that highlight the deepest Western deeping fault (Figure 1). The yellow boxes highlight structures that are consistent between the images created from synthetic and field DASV. Figure 3b also contains a red box that denotes a possible coherent event in the data from Brady that doesn't coincide with a fault included in the synthetic modeling.

Figures 4a and 4b contain the P-S images for both the synthetic 4-fault model and the Brady DASV field data respectively. These slices focus on the middle, Western-dipping fault, where the three yellow boxes highlight the most promising features. In the crossline slice (lower right), the fault demonstrates a long coherent structure in both 4a and 4b. The middle western-dipping fault is a coherent, 200m-long feature (310 to 550m depth). From probing the 3D cubes, it was discovered that this fault is well image for 400m along strike.

In the depth slice (upper left) of both images in Figure 4, the focusing effect of the velocity model is seen in just neighboring the middle West-dipping fault. Focusing is also seen in

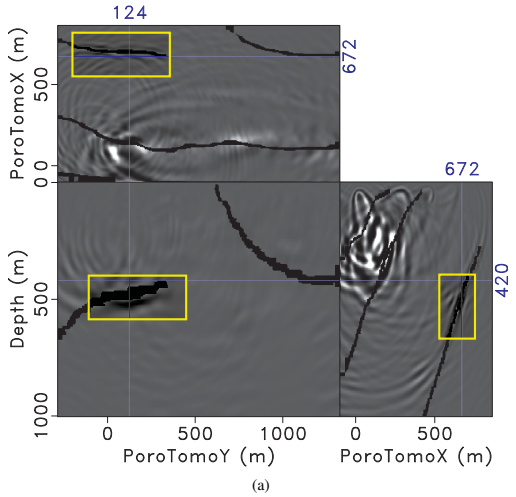

Figure 3: P-P images for synthetic 4 fault model (a) and of the DAS data (b) highlighting consistency around the deepest Western dipping fault in yellow boxes

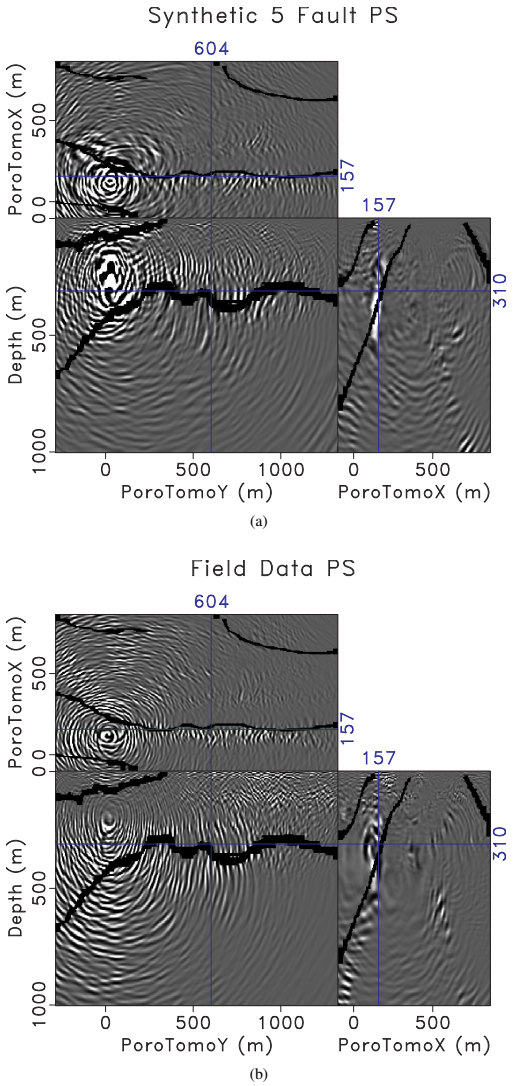

Figure 4: P-S images for synthetic 4 fault model (a) and of the DAS data (b) highlighting consistency around the middle Western dipping fault in yellow boxes

the PoroTomoX and PoroTomoY panels. In the lower right panels, there are brighter spots that begin at PoroTomoX=500 and depth=500, which coincide with a higher velocity structure (4,500m/s versus 4,000m/s). There are also focusing patterns below the yellow box in the lower left panels.

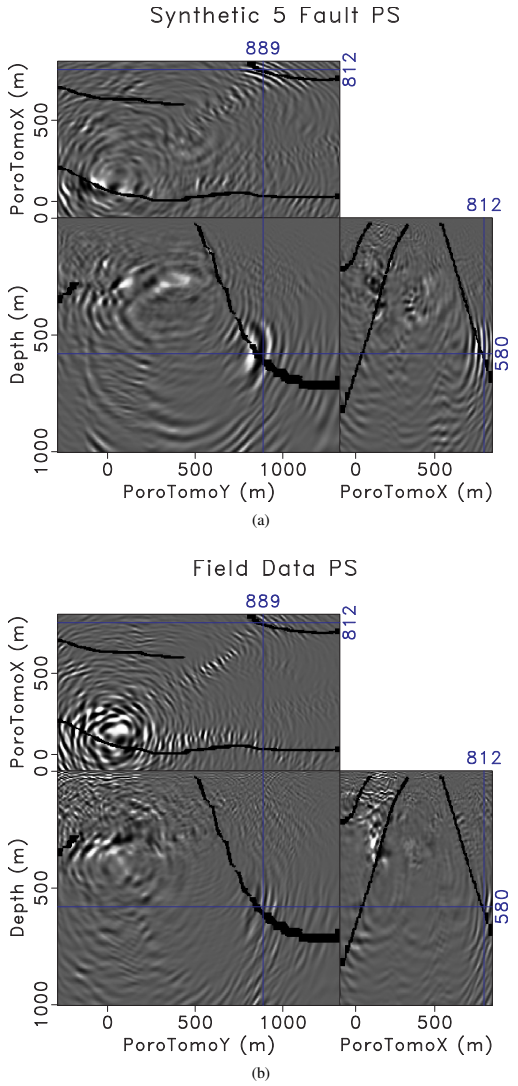

Figure 5: P-S images for synthetic 4 fault model (a) and of the DAS data (b) highlighting consistency around the far Eastern dipping fault in yellow boxes

QUANTIFYING INFORMATION CONTENT IN RTM IMAGES

Important to this work is comparing the information recovered from point sensors versus or in combination with the DAS fibers (Jreij et al., 2018). Specifically of interest is to utilize the value of information metric to statistically quantify how reliable information sources are at recognizing important subsurface parameters (Trainor-Guitton, 2014). The combination of machine learning algorithms and computer vision techniques could make it possible to discriminate between migration artifacts and actual events caused by subsurface structures.

Fault Classification via Convolutional Neural Networks

Machine learning techniques can detect weak or complex patterns not discernible by the human eye. In this particular case, strong migration artifacts may make it harder to discern weaker coherent patterns that may be attributed to important subsurface features, e.g. faults and stratigraphy. This work uses convolutional neural networks (CNN) which have the advantage of not requiring *a priori* information, pre-processing nor selecting of features. The Inception-v3 model is a CNN that has been trained and tested to match or exceed human ability to detect complex objects from 2D images (Szegedy et al., 2015). The original Inception-v3 model was tested on the 2012 ImageNet Large Scale Visual Recognition Challenge (Russakovsky et al., 2015). The training dataset consisted of millions of labeled images that depicted over 1,000 object categories. Thus, the Inception-v3 model utilizes a transfer learning approach by utilizing the ImageNet repository and applying the pre-trained CNN model on different problems such as our fault imaging application. We can therefore take advantage of the CNN that can detect edges, shapes, and other high level features to help with classifying fault versus not fault in our noisy images.

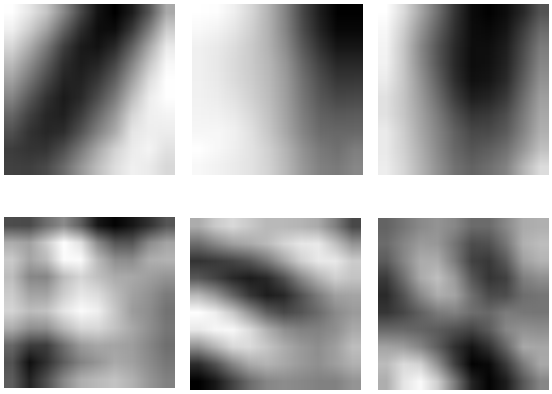

Figure 6: Examples from DASV data. Top row: 3 examples of "fault" training data. Bottom row: 3 examples of "not fault" training data

To add training and testing images specific to this classification problem, 2D slices were scanned with a 10 by 10 template but then resampled to the inception expected size (299x299). Using either the flat reflector or Brady fault model, the training data were classified as fault or no fault. Figure 6 shows 3 examples of each for the DASV scenario. The images from flat reflectors were limited to the -100/+700m in the PoroTomoY and only the top two reflectors. For the two non-flat scenarios (images created by synthetic 4-fault reflectivity and the field DAS data), only three crossline sections were used to generate fault and not fault samples. Specifically, the crosslines shown in the lower right of Figures 3, 4 and 5 for both the synthetic and field cases were used and produced on the order of

3,300 fault and 80,000 not fault samples. From this large pool, the samples were randomly down-sampled unequally in order to have adequate representation of both classifications. About 700 fault samples and 1,600 Not Fault samples were selected for a 30/70% fault/not fault split.

Preliminary classification results for the 4 flat reflector images are summarized in Table 1. The false negatives are high (54.6%). This is likely due to the training data having fault classification given for the two layers (in between the pair of reflectors), and not just at the four reflectors. This should be modified such that the fault is classified only where the reflectivity contrast exists.

4 Flat Reflectors		Predicted (*Interpreted*) $\tilde{\Theta}_j$ Fault	Predicted (*Interpreted*) $\tilde{\Theta}_j$ No Fault
Actual Θ_i	Fault	729 (45.4%)	878 (54.6%)
	No Fault	11 (0.23%)	4,672 (99.77%)

Table 1: 4 Flat Reflectors: Classification of faults and no faults.

The preliminary classification results for the images generated by synthetic data of the Brady 4 fault model as reflectors are summarized in Table 2. The false negatives is about the same percentage as the the four flat reflectors (Table 1). However, now there are significant percentage of false positives: 14.8%. This is can be attributed to the increase in artifacts inadvertently included in the training data, given the more complex geometry compared to the flat reflector scenario.

Brady 4 Fault Reflectors		Predicted (*Interpreted*) $\tilde{\Theta}_j$ Fault	Predicted (*Interpreted*) $\tilde{\Theta}_j$ No Fault
Actual Θ_i	Fault	470 (43.2%)	616 (56.7 %)
	No Fault	201 (14.8%)	1,155 (85.2%)

Table 2: Brady 4 Fault Reflector: Classification of faults and no faults.

Table 3 contains the preliminary classification results for the DASV field data. The true positives (59.4%) are higher than in Table 2, possibly because the alignment of the fault locations (the Siler & Faulds model) may align better with the amplitude contrast. However, the false positives (24.8%) is higher than the two previous synthetic cases.

RTM from DASV data		Predicted (*Interpreted*) $\tilde{\Theta}_j$ Fault	Predicted (*Interpreted*) $\tilde{\Theta}_j$ No Fault
Actual Θ_i	Fault	199 (59.4%)	136 (40.6 %)
	No Fault	472 (24.8%)	1,430 (75.2%)

Table 3: RTM from DAS data: Classification of faults and no faults.

CONCLUSIONS AND DISCUSSION

The training sets in all three scenarios are generated by comparing locations of the "fault" and the collocated patterns in the RTM image. For thick "faults" the middle of fault does not represent any contrast or reflectivity, and thus will not produce a coherent event in the RTM image. However, this location will be classified as a fault. Thus, to improve this training, a gradient of the reflectivity should be used instead. This may align better in space with the RTM events that are consistent with fault reflectivity. Future work will improve the classification, and also investigate the inline 2D sections of the Brady fault scenario.

A large advantage of the CNN models is avoiding the feature selection step. However, quality control of the training dataset is still of the utmost importance and will affect results. The largest limitation of the Inception v3 is its inability to accept 3D images. Guitton (2018) describes a CNN model designed specifically for 3D seismic images.

Using the CNN classifier as a technique to achieve a relative comparison of two images is useful since it is quantitative and interpreter-agnostic. Most importantly it is statistical: providing a measure of information content that could be utilized in a value of information relative comparison for the synthetic and DAS image case. Besides training and testing, a multi-fold approach should be used for model evaluation.

ACKNOWLEDGMENTS

The work presented herein was funded in part by the Office of Energy Efficiency and Renewable Energy (EERE), U.S. Department of Energy, under Award Numbers DE-EE0006760 and DE-EE0005510.